

EDINBURGH  
INSTRUMENTS





# PRECISION RAMAN

Best-in-class Raman microscopes  
for research and analytical requirements  
backed with world-class customer  
support and service.



[edinst.com](http://edinst.com)

# Correlation of crystal violet biofilm test results of *Staphylococcus aureus* clinical isolates with Raman spectroscopic read-out

Christina Ebert<sup>1,2</sup> | Lorena Tuchscher<sup>2,3</sup>  | Nancy Unger<sup>1,2</sup> |  
Christine Pöllath<sup>2,3</sup> | Frederike Gladigau<sup>1,4</sup> | Jürgen Popp<sup>1,2,4</sup> |  
Bettina Löffler<sup>2,3</sup> | Ute Neugebauer<sup>1,2,4</sup> 

<sup>1</sup>Leibniz Institute of Photonic Technology, Jena, Germany

<sup>2</sup>Center for Sepsis Control and Care, Jena University Hospital, Jena, Germany

<sup>3</sup>Institute for Medical Microbiology, Jena University Hospital, Jena, Germany

<sup>4</sup>Institute of Physical Chemistry and Abbe School of Photonics, Friedrich Schiller University Jena, Jena, Germany

## Correspondence

Ute Neugebauer, Institute of Physical Chemistry and Abbe School of Photonics, Friedrich Schiller University Jena, Helmholtzweg 4, Jena D-07743, Thuringia, Germany.  
Email: ute.neugebauer@leibniz-ipht.de

## Funding information

European Union, Grant/Award Number: 861122; Leibniz Association, Grant/Award Number: W8/2018; Bundesministerium für Bildung und Forschung (BMBF), Grant/Award Number: FKZ 01EO1502

## Abstract

Biofilm-related infections occur quite frequently in hospital settings and require rapid diagnostic identification as they are recalcitrant to antibiotic therapy and make special treatment necessary. One of the standard microbiological in vitro tests is the crystal violet test. It indirectly determines the amount of biofilm by measuring the optical density (OD) of the crystal violet-stained biofilm matrix and cells. However, this test is quite time-consuming, as it requires bacterial cultivation up to several days. In this study, we correlate fast Raman spectroscopic read-out of clinical *Staphylococcus aureus* isolates from 47 patients with different disease background with their biofilm-forming characteristics. Included were low ( $OD < 10$ ), medium ( $OD \geq 10$  and  $\leq 20$ ), and high ( $OD > 20$ ) biofilm performers as determined by the crystal violet test. Raman spectroscopic analysis of the bacteria revealed most spectral differences between high and low biofilm performers in the fingerprint region between 750 and 1150  $\text{cm}^{-1}$ . Using partial least square regression (PLSR) analysis on the Raman spectra involving the three categories of biofilm formation, it was possible to obtain a slight linear correlation of the Raman spectra with the biofilm OD values. The PLSR loading coefficient highlighted spectral differences between high and low biofilm performers for Raman bands that represent nucleic acids, carbohydrates, and proteins. Our results point to a possible application of Raman spectroscopy as a fast prediction tool for biofilm formation of bacterial strains directly after isolation from the infected patient. This could help clinicians make timely and adapted therapeutic decision in future.

Dedicated to Derek A. Long, one of the pioneers of Raman spectroscopy.

This is an open access article under the terms of the Creative Commons Attribution-NonCommercial License, which permits use, distribution and reproduction in any medium, provided the original work is properly cited and is not used for commercial purposes.

© 2021 The Authors. *Journal of Raman Spectroscopy* published by John Wiley & Sons Ltd.

**KEYWORDS**

biofilm, partial least square regression (PLSR), patient isolates, Raman spectroscopy, *Staphylococcus aureus*

## 1 | INTRODUCTION

*Staphylococcus aureus* is one of the most frequent pathogens associated with nosocomial infections. Approximately 30% of the human population is asymptotically and permanently colonized with *S. aureus* in the nasopharyngeal area.<sup>[1]</sup> However, *S. aureus* is also able to cause severe invasive infections such as sepsis that needs fast diagnosis and treatment. Chronic infections with *S. aureus* are difficult to treat and often related to biofilm formation.

Biofilms are aggregates of microorganisms that attach to each other or adhere to a surface and produce a hydrated matrix composed of extracellular polymeric substances (EPS).<sup>[2]</sup> This matrix gives stability and a specific organized structure. It is mainly composed of polysaccharides, proteins, lipids, and extracellular DNA.<sup>[2]</sup> Although giving protection from antimicrobial substances and the immune system, biofilms are not a static microbial community but are undergoing continued remodeling through shedding of planktonic bacteria that are able to colonize different parts of the body.<sup>[2]</sup> To treat biofilm-forming bacteria, often up to 1000 times higher doses of antibiotics are necessary than treating the planktonic form.<sup>[3]</sup>

*S. aureus* produces the polysaccharide intercellular adhesin (PIA), a poly- $\beta$ (1–6)-*N*-acetylglucosamine, as the main polysaccharide of the EPS.<sup>[4,5]</sup> However, strains exist that are able to form biofilms independently of PIA gene expression thereby producing alternative forms of biofilms with mainly protein-based composition.<sup>[5]</sup> Thus, biofilm composition and production may differ a lot between *S. aureus* strains.

The importance of biofilm-related infections of *S. aureus* for hospital settings is emphasized by the recognition that biofilm infections cause around 80% of all infections.<sup>[6]</sup> Even more importantly, they are difficult to treat, because antimicrobial therapy alone is not effective. Often, the only option is to prevent *S. aureus* biofilms from forming or to surgically remove them.<sup>[6]</sup>

An important example for such a difficult-to-treat infection with *S. aureus* is osteomyelitis, a chronic infection and inflammation of bone tissue resulting in severe and painful bone loss. Osteomyelitis can derive from hematogenous spread from the blood stream (hematogenous osteomyelitis) or is associated with inoculation directly from outside, for example, through surgery of implants (nonhematogenous osteomyelitis).<sup>[6]</sup>

Because of the high significance of biofilm infections in hospital settings, fast and easy diagnostic methods to identify pathogenic *S. aureus* strains that have higher potential for biofilm production are needed. The standard method for identification of biofilm producing strains in vitro is staining of the biofilm with crystal violet that stains negatively charged molecules on the cells and in the EPS, followed by measurement of the optical density (OD).<sup>[7–9]</sup> Indeed, plenty of different stains for specific biofilm molecules exist, which can be analyzed using spectrophotometric or microscopic techniques.<sup>[9–13]</sup> However, all of these methods are quite laborious and time consuming due to the necessity of growing the biofilm in vitro before analysis. Therefore, these methods cannot be applied in routine diagnostic.

Raman spectroscopy offers the advantage of being label-free, fast, and contact-free, therefore allowing to obtain very specific fingerprint spectra of the sample in a noninvasive way. This spectral information can be used—in combination with statistical methods—to identify bacterial species and strains.<sup>[14]</sup> Raman spectroscopy was successfully applied not only to study clinical relevant microbial biofilms, for example, for chemical analysis of biofilm formation and composition,<sup>[15–27]</sup> but also to identify different bacterial species forming biofilms and to discriminate between biofilm-positive and -negative strains.<sup>[28–31]</sup> Additionally, the interaction of antibiotics with biofilms and their efficacy has been evaluated with Raman spectroscopy.<sup>[32–34]</sup>

Here, we applied Raman microspectroscopy on diverse *S. aureus* clinical isolates from patients with different disease background that showed low, medium, or high biofilm production in vitro. At least 10 strains were selected for each biofilm group. Our aim was to prove if the information of the Raman spectra of bacteria grown in liquid culture could be correlated to the biofilm production level obtained from classical crystal violet microbiological test values. This could pave the way to predict biofilm formation independent of time-consuming biofilm cultivation. The prediction of the grade of biofilm production might help to detect *S. aureus* biofilm infections in patients and identify patients at high risk in hospital settings and to plan an adequate successful therapy using antibiotics that are active against the biofilm form of the bacterial species.

## 2 | MATERIAL AND METHODS

### 2.1 | *S. aureus* strains

Forty-seven *S. aureus* clinical isolates from a previous study<sup>[35]</sup> have been used here (Table 1). The isolates originated from nasal colonization of healthy donors and from patients with hematogenous osteomyelitis, with endoprosthesis infection (nonhematogenous osteomyelitis) as well as from sepsis patients. Isolation protocols have been published.<sup>[35]</sup>

### 2.2 | Biofilm production analysis

Biofilm production was measured by the classical microbiological crystal violet test on cultured biofilms in microtiter plates.<sup>[36]</sup> First, bacteria were grown overnight in Tryptic Soy Bean broth (TSB, Carl Roth, Germany) with 0.25% glucose at 160 rpm and 37°C. *S. epidermidis* strain RP62A was used as positive control. A microtiter plate containing TSB with 0.25% glucose was inoculated with overnight culture at a dilution of 1:200 and incubated at 37°C for 24 h for in vitro biofilm formation.

For analysis of biofilm production, the medium was removed from the wells and washed twice with phosphate-buffered saline (PBS). Thereafter, 1% crystal violet solution was added and incubated for 10 min. After washing three times with PBS, the bacteria biofilm was incubated with a mixture of 80% ethanol and 20% acetone (4:1) for 10 min. Absorbance was measured at 570 nm at four different locations per well in an enzyme-linked immunosorbent assay (ELISA) reader (Tecan infinite 200Pro).

### 2.3 | Cultivation procedure for Raman spectroscopic measurement

The cultivation of the strains should be conducted in a similar way like the crystal violet biofilm assay but without long-term cultivation for biofilm formation. Therefore, the bacterial strains were grown in TSB at 160 rpm and 37°C using an overnight culture for inoculation with an OD of 0.05. After 3 h, the OD<sub>600</sub> of all cultures was measured. The time point of 3 h was chosen to generate highly homogeneous bacterial culture to avoid metabolic growth phase-related spectral differences as reported previously.<sup>[37,38]</sup> As seen in Table 1, bacteria have a generation time of 30–40 min; thus, after 3 h, bacteria are in the exponential growth phase. If the OD<sub>600</sub> was 2 or higher, 4 ml of culture was used for sample preparation. If the OD<sub>600</sub> was less

than 2, the volume of culture used for sample preparation was 8 ml to obtain a comparable amount of bacteria. Samples were centrifuged at 3.500×g for 5 min, and the obtained pellets were washed twice with 1 ml fresh PBS. Finally, the bacterial pellets were resuspended in 4% formaldehyde (Histofix, Carl Roth, Germany) and fixed for 10 min at room temperature (RT). After another centrifugation step, the fixative was removed completely, and the pellets were resuspended in deionized water and stored at –80°C.

### 2.4 | Raman spectroscopic measurement

Fixed bacterial samples were centrifuged by using a Cytospin centrifuge (Hettich, Germany) onto CaF<sub>2</sub> slides (Crystal, Germany) coated with 0.2% gelatin in order to obtain a uniform bacterial layer and to ensure good attachment for bulk measurement. The samples were characterized with an alpha300R Raman spectrometer (WITec, Germany) in PBS buffer using a 60× water immersion objective (NA 1.0, Nikon) and a 532-nm Nd:YAG laser at 15 mW. A 100-μm multimode fiber was used to collect the light scattered from the bacteria. Excitation wavelength of 532 nm was chosen, as it is available in many commercial Raman devices and thus could be used for potential later translation. In addition, extensive databases for the identification of bacteria have been recorded previously with this wavelength.<sup>[39,40]</sup>

Spectra were recorded of each strain on different spatial positions of the sample using an integration time of 5 s/spectrum and one accumulation. One spectrum was recorded per position to give a total of 32–38 spectra per strain from the 32–38 different positions. For 47 strains, this results in a total number of 1570 Raman spectra. After preprocessing, 1529 spectra were included in the final analysis.

### 2.5 | Data analysis with R

The software Gnu R (R Core Team (2018): R, a language and environment for statistical computing. R Foundation for Statistical Computing, Vienna, Austria (R version 3.4.4 [2018-03-15] and 4.0.2 [2020-06-22]), was used for statistical analysis of the Raman spectra.

Used packages are as follows:

- hyperSpec (hyperSpecJSS. Claudia Beleites and Valter Sergio: `hyperSpec: a package to handle hyperspectral data sets in R', R package versions 0.99-20171005 and 00.99-20200527. <https://github.com/cbeleites/hyperSpec>).

**TABLE 1** Strains used in this study and the according information about disease, generation time, crystal violet test results, and biofilm formation level

Strain name	Disease of patient where strain was isolated from	Generation time in min ( $n = 3$ ) <sup>[a]</sup>	Biofilm formation OD value (crystal violet test)	Biofilm formation level <sup>[b]</sup>
N14	Nasal colonization	30.68	0.7	Low
D2	Hematogenous osteomyelitis	31.81	1.7	Low
Hawa51	Nonhematogenous osteomyelitis	41.28	4	Low
N13	Nasal colonization	30.75	4	Low
Ilun61	Sepsis	30.74	4	Low
Edbr39	Hematogenous osteomyelitis	30.8	4.5	Low
Hebl44	Hematogenous osteomyelitis	30.85	4.7	Low
N15	Nasal colonization	31.74	5	Low
Hewi37	Sepsis	31.17	5	Low
Hegl68	Hematogenous osteomyelitis	31.07	5.3	Low
N1	Nasal colonization	31.18	6	Low
D3	Hematogenous osteomyelitis	31.29	7.7	Low
Hafa83	Nonhematogenous osteomyelitis	31.89	8.3	Low
Chwa42	Hematogenous osteomyelitis	31.00	9	Low
Mabö56	Sepsis	30.48	9	Low
Udmi62	Sepsis	30.72	9	Low
Genä42	Sepsis	31.26	10	Medium
S6	Sepsis	31.74	10.8	Medium
Reho41	Sepsis	31.30	12.7	Medium
M6	Nonhematogenous osteomyelitis	32.07	13	Medium
D1	Hematogenous osteomyelitis	31.05	14.2	Medium
Rahe58	Hematogenous osteomyelitis	31.33	14.3	Medium
M3	Nonhematogenous osteomyelitis	31.03	14.4	Medium
N9	Nasal colonization	34.17	14.6	Medium
Hapo37	Nonhematogenous osteomyelitis	31.27	15	Medium
M4	Nonhematogenous osteomyelitis	31.14	15.4	Medium
N7	Nasal colonization	31.49	15.8	Medium
N8	Nasal colonization	30.84	15.8	Medium
N11	Nasal colonization	31.22	16.2	Medium
N4	Nasal colonization	30.73	16.4	Medium
N6	Nasal colonization	31.29	18.7	Medium
Reju49	Nonhematogenous osteomyelitis	31.29	20	Medium
O1	Hematogenous osteomyelitis	30.93	20	Medium
M1	Nonhematogenous osteomyelitis	30.37	20	Medium
M2	Nonhematogenous osteomyelitis	32.03	20	Medium
M5	Nonhematogenous osteomyelitis	31.36	21	High
N12	Nasal colonization	31.93	21.6	High
M7	Nonhematogenous osteomyelitis	33.56	22.2	High
S1	Sepsis	31.21	22.6	High
Josc25	Hematogenous osteomyelitis	32.88	23.3	High
O3	Hematogenous osteomyelitis	31	23.5	High

(Continues)

TABLE 1 (Continued)

Strain name	Disease of patient where strain was isolated from	Generation time in min ( $n = 3$ ) <sup>[a]</sup>	Biofilm formation OD value (crystal violet test)	Biofilm formation level <sup>[b]</sup>
O2	Hematogenous osteomyelitis	31.01	24.4	High
Jüze47	Nonhematogenous osteomyelitis	30.67	25.3	High
N10	Nasal colonization	30.69	26	High
Ankö60	Sepsis	30.99	26.3	High
Kak154	Sepsis	31.13	30.1	High
O4	Hematogenous osteomyelitis	30.87	33.8	High

<sup>a</sup>Generation times were calculated from growths curves. Please notice that only the strain Hawa51 showed a high generation time indicating that this strain is growing slower in comparison to other strains. The generation time is calculated as indicated in the previous publication.<sup>[48]</sup>

<sup>b</sup>An OD value < 10 represents low biofilm formation, an OD  $\geq$  10 and  $\leq$  20 normal (medium) biofilm formation, and an OD value of >20 high biofilm formation.

- pls (Bjørn-Helge Mevik, Ron Wehrens and Kristian Hovde Liland [2020]. pls: Partial Least Squares and Principal Component Regression. R package version 2.7–3. <https://CRAN.R-project.org/package=pls>).
- rjava (Simon Urbanek [2017]. rJava: Low-Level R to Java Interface. R package version 0.9–9. <https://CRAN.R-project.org/package=rJava>).
- Xlsx (Adrian A. Dragulescu [2014]. xlsx: Read, write, format Excel 2007 and Excel 97/2000/XP/2003 files. R package version 0.5.7. <https://CRAN.R-project.org/package=xlsx>).

Raman spectra with cosmic rays were removed from the data set before preprocessing. Remaining spectra were baseline corrected using a polynomial fifth order. Based on Makki et al., all partial least square regression (PLSR) data analyses were performed without normalization.<sup>[41]</sup> For calculating the root mean squared error of calibration (RMSEC) values, tenfold cross-validation was performed; that is, the data set was split into training and test data. In order to avoid weighting due to the slightly different number of spectra per strain, every 10th spectrum was used for the test data set. After the splitting, PLSR was performed with the training data set, and the prediction of the test data set was used for calculating the RMSEC value. The root mean squared error of cross-validation (RMSECV) values were calculated with leave-one-strain-out cross validation. The root mean squared error of prediction (RMSEP) values were calculated based on the data splitting used for the RMSECV. The prediction was calculated for each spectrum in the test data set individually and used for calculating the RMSEP values of this strain data set. To calculate the leave-one-spectrum-out PLSR of the recorded spectra as validation, 10 PLSR components were used, because of the smallest error before the plateau occurs in the RMSEC (Figure S1a) and

RMSECV (Figure S1b) and the most stable region in the RMSEP (Figure S1c).

## 3 | RESULTS

### 3.1 | In vitro biofilm formation analysis

Biofilm formation of 47 *S. aureus* clinical isolates was assessed in vitro using classical crystal violet method. Results are presented in Table 1. The *S. aureus* isolates originated from patients with four different disease backgrounds, that is sepsis, hematogenous osteomyelitis, nonhematogenous osteomyelitis as well as nasal colonization in healthy donors. It can be seen in Table 1 and Figures S3–S5 that the disease background does not influence the biofilm formation level. In this manuscript strains with OD values less than 10 in the crystal violet assay are referred as low biofilm producers, strains with OD between 10 and 20 as medium biofilm producers, and strains with OD higher than 20 as high biofilm producers. Low, medium, and high biofilm producers were identified in each disease group indicating that the level of biofilm production was not correlated to a specific pathology.

### 3.2 | Raman spectroscopic analysis

Raman spectra were recorded of each strain after a short cultivation time of 3 h in liquid culture under optimal nutrient conditions. Figure 1 shows a representative mean Raman spectrum of a low biofilm producer, *S. aureus* Hawa51 with OD 4 in crystal violet test, a high biofilm producer, *S. aureus* Kak154 with OD 30.1 in the crystal violet test, and the two *S. aureus* strains Genä42 and M5 with ODs in crystal violet test between

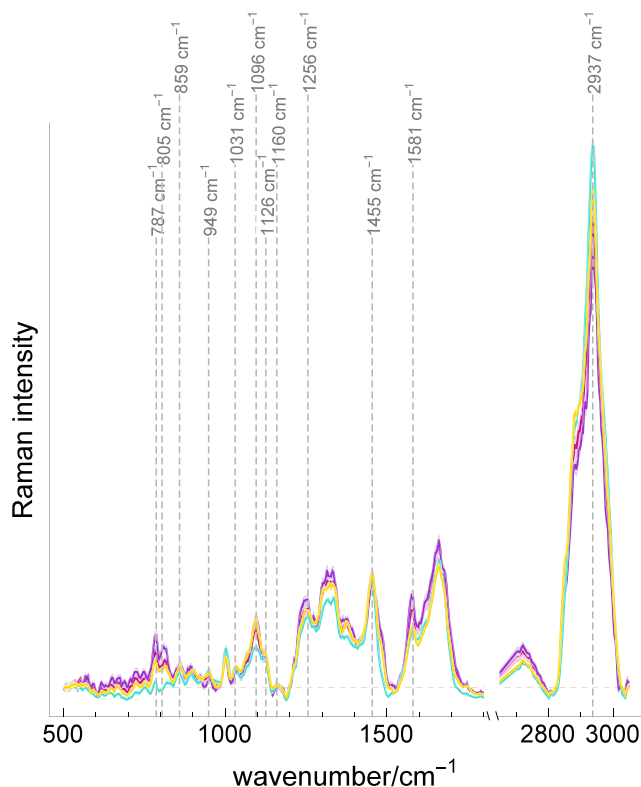


**FIGURE 1** Representative Raman spectra with standard deviation of four *Staphylococcus aureus* strains from different optical density (OD) regions. Depicted are the normalized and base line corrected mean spectra with standard deviation of *S. aureus* strain Kak154 (—, turquoise), a high biofilm producer with an OD of around 30 in the crystal violet test, *S. aureus* Hawa51 (—, purple), a low biofilm producer giving an OD value of 4 in the crystal violet test, *S. aureus* strain Genä42 (—, yellow), an intermediate biofilm producer with a OD value of 10 in the crystal violet test and as the second intermediate biofilm producer with an OD of 21 in the crystal violet test the *S. aureus* strain M5 (—, red)

10 (Genä42) and 21 (M5), for first comparison. To assess the reproducibility and repeatability of the Raman measurements for each strain, the relative standard deviation (RSD) was calculated. The mean of all RSD is on average at 0.12 as can be seen in Figure S2. Mean Raman spectra with standard deviation of all investigated strains are shown in Figures S3–S5.

Typical Raman bands of the biological components of bacteria can be seen in the spectra, such as vibrational bands of nucleic acid components at  $787\text{ cm}^{-1}$  (purine bases cytosine, thymine, and uracil<sup>[25,30,42]</sup>), at  $805\text{--}810\text{ cm}^{-1}$  (RNA backbone stretching<sup>[20]</sup>), at  $1581\text{ cm}^{-1}$  (pyrimidine bases guanine and adenine<sup>[20,25,42]</sup>), and at  $1096\text{ cm}^{-1}$  ( $\text{PO}_2^-$  stretching<sup>[20,25,30,42]</sup>). Interestingly, those bands had decreased relative intensity in the high biofilm producer strain *S. aureus* Kak154 (Figure 1). In

contrast, bands prominent in proteins such as the phenylalanine ring breathing mode ( $1001\text{ cm}^{-1}$ )<sup>[20,25,30,42]</sup> and the  $\text{CH}_2$  deformation band ( $1455\text{ cm}^{-1}$ )<sup>[20,42]</sup> were increased in *S. aureus* Kak154 compared with the low biofilm producer strain *S. aureus* Hawa51. Other protein bands such as the amide I ( $1661\text{ cm}^{-1}$ )<sup>[20,42]</sup> and the amide III ( $1256\text{ cm}^{-1}$ )<sup>[20,25,42]</sup> bands revealed similar relative intensities in all four strains. Most strikingly, Raman band intensities in the region of  $850\text{--}1050\text{ cm}^{-1}$  representing likely polysaccharide bands<sup>[17,42]</sup> such as the C—O—C 1,4 glycosidic link ( $858\text{ cm}^{-1}$ ),<sup>[42]</sup> the C—O—C glycosidic bond ring ( $949\text{ cm}^{-1}$ ),<sup>[30]</sup> and the C—O stretching band ( $1031\text{ cm}^{-1}$ )<sup>[16]</sup> had higher relative intensities in the high biofilm producer strain *S. aureus* Kak154. Furthermore, the C—O—C 1,4 glycosidic link band ( $1126\text{ cm}^{-1}$ )<sup>[42]</sup> also showed increased relative intensity. In contrast, other carbohydrate bands outside this wavenumber region such as the C—O—C glycosidic link symmetric ring breathing ( $1096\text{ cm}^{-1}$ )<sup>[16,25,42]</sup> and the C—C and C—O asymmetric ring breathing ( $1160\text{ cm}^{-1}$ )<sup>[16,42]</sup> showed lower relative intensities in Kak154 compared with *S. aureus* Hawa51, Genä42, and M5.

Most differences in the Raman spectra of high and low biofilm producer strains were apparently identified in the region of  $750\text{--}1150\text{ cm}^{-1}$  (Figures 1 and S3) and reveal important differences in polysaccharide amount, the main macromolecule present in biofilm EPS.

### 3.3 | PLSR analysis of Raman data

PLSR analysis was performed to visualize a possible correlation between OD value in the crystal violet test, that is, the biofilm formation, and the Raman spectroscopic signature. PIA-based biofilm would result in higher relative intensities of the carbohydrate Raman bands. The scatter plot of the leave-one-spectrum-out PLSR-predicted OD values against the crystal violet test OD values is shown in Figure 2. A linear correlation between the OD values and the Raman spectral signatures of the analyzed *S. aureus* strains independently of their disease background could be seen by the simultaneous increase of the predicted OD values and the OD value obtained from the crystal violet tests supported by the calculated correlation factor of 0.67.

The loadings are displayed for all 10 used PLSR components in Figure 3 (left) and reveal differences between the strains at band positions 787, around 805 (nucleic acids), and at  $849\text{ cm}^{-1}$  (likely corresponding to the  $858\text{ cm}^{-1}$  C—O—C 1,4 glycosidic link band in Figure 1), 949, 1031, and  $1126\text{ cm}^{-1}$  (carbohydrates) as well as

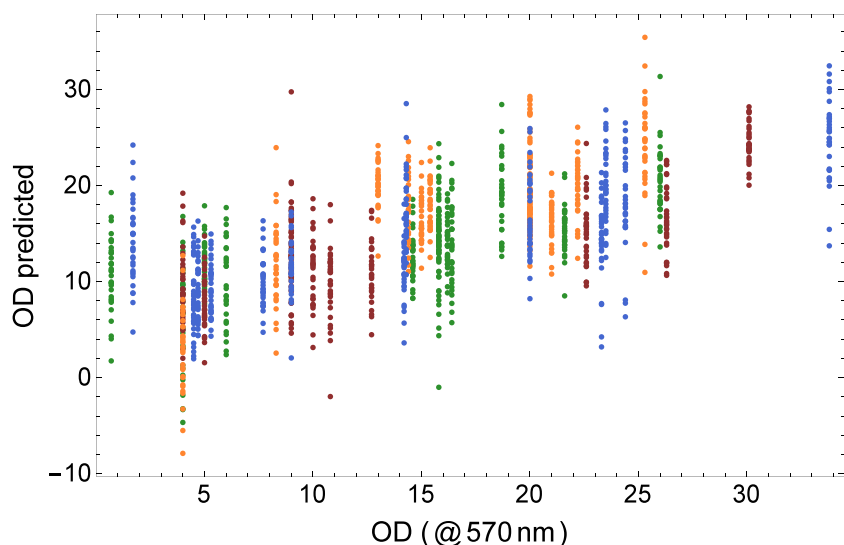


**FIGURE 2** Correlation of the partial least square regression (PLSR)-predicted optical density (OD) values with biofilm production values. Depicted are the OD values predicted by the leave-one-spectrum-out PLSR against the experimental biofilm OD values from the crystal violet biofilm test. Each vertical line represents one strain with the single Raman spectra represented as single dots, whereas the color indicates the disease background of the strains (● blue, hematogenous osteomyelitis; ● green nasal colonization; ● orange nonhematogenous osteomyelitis; ● brown, sepsis)

around  $1004\text{ cm}^{-1}$  (phenylalanine). Loadings 1–3 show the best correlation between OD and PLSR scores as depicted in Figure 3 (right). The negative and positive bands at the described positions indicate that high biofilm formation correlates with increased Raman signals for carbohydrates and proteins but reduced Raman bands of nucleic acids.

## 4 | DISCUSSION

Biofilm-associated infections have drawn increasing attention in the last decades because they are difficult to diagnose and antibiotic treatment very often fails to eradicate the infection. Principally, this is not because of antibiotic resistant bacteria, but rather due to the complex composition and structure of biofilms making antibiotic penetration difficult.<sup>[2]</sup> Additionally, the bacteria can be in a dormant metabolic state thereby showing phenotypic resistance/tolerance.<sup>[2]</sup> As a consequence, many of the standard antibiotic classes used to treat the planktonic form of the bacteria will not work against the same species in the dormant form within the biofilm or need at least much higher doses.<sup>[3]</sup> Therefore, it is of utmost importance to detect bacterial biofilms in infected patients. Some bacterial strains have a higher capability to grow as biofilms in vitro than others. Although we cannot be sure that the strains with high biofilm forming capability in vitro would behave the same as in vivo, it still would be desirable to have a rapid in vitro tool for prediction if the bacterial strain responsible for the infection will have a high probability to form biofilm or not. This could help to improve diagnostic and treatment options by guiding to a suitable antimicrobial therapy in advance.

Here, we explored the potential of Raman spectroscopy as a fast and label-free technology to predict biofilm production capability using clinical isolates of 47 different *S. aureus* strains with low, medium, and high biofilm production capability. A possible correlation between the biochemical information of the Raman spectra signatures with OD experimental values obtained from in vitro grown biofilms was found using PLSR analysis. This correlation was independent of the disease background from which the strains were isolated.

Three carbohydrate bands ( $849$ ,  $949$ , and  $1031\text{ cm}^{-1}$ ) were found to be positively correlated with the in vitro formation of biofilms. Carey et al.<sup>[20]</sup> and Samek et al.<sup>[30]</sup> also reported an increase in the band intensity near  $950\text{ cm}^{-1}$  in *S. epidermidis* biofilm compared with planktonic phase. In biofilms formed by Gram-negative strains such as *Escherichia coli*, *Klebsiella pneumoniae*, and *Pseudomonas aeruginosa*, a higher intensity of those bands was found in comparison with the planktonic form as well.<sup>[17]</sup> Generally, the wavenumber region of  $700$ – $950\text{ cm}^{-1}$  is representing side group deformations in different carbohydrates that were measured as references.<sup>[42]</sup> These bands were also observed in a Raman spectroscopic study of different oral biofilms caused by cariogenic streptococci.<sup>[26]</sup> Also, we additionally observed an increased intensity of the  $1126\text{ cm}^{-1}$  carbohydrate band in high biofilm formers. This band frequently showed a higher intensity in other biofilms as well, such as in *P. aeruginosa* biofilms,<sup>[16–18,21]</sup> the bacterial species that is most studied for biofilms, and in biofilms from *E. coli* and *K. pneumoniae*.<sup>[17]</sup>

The nucleic acid bands at  $787$  and  $805\text{ cm}^{-1}$  were found to have a negative correlation with the in vitro biofilm OD values in our PLSR. This likely reflects a reduced metabolism in the bacteria that results in less



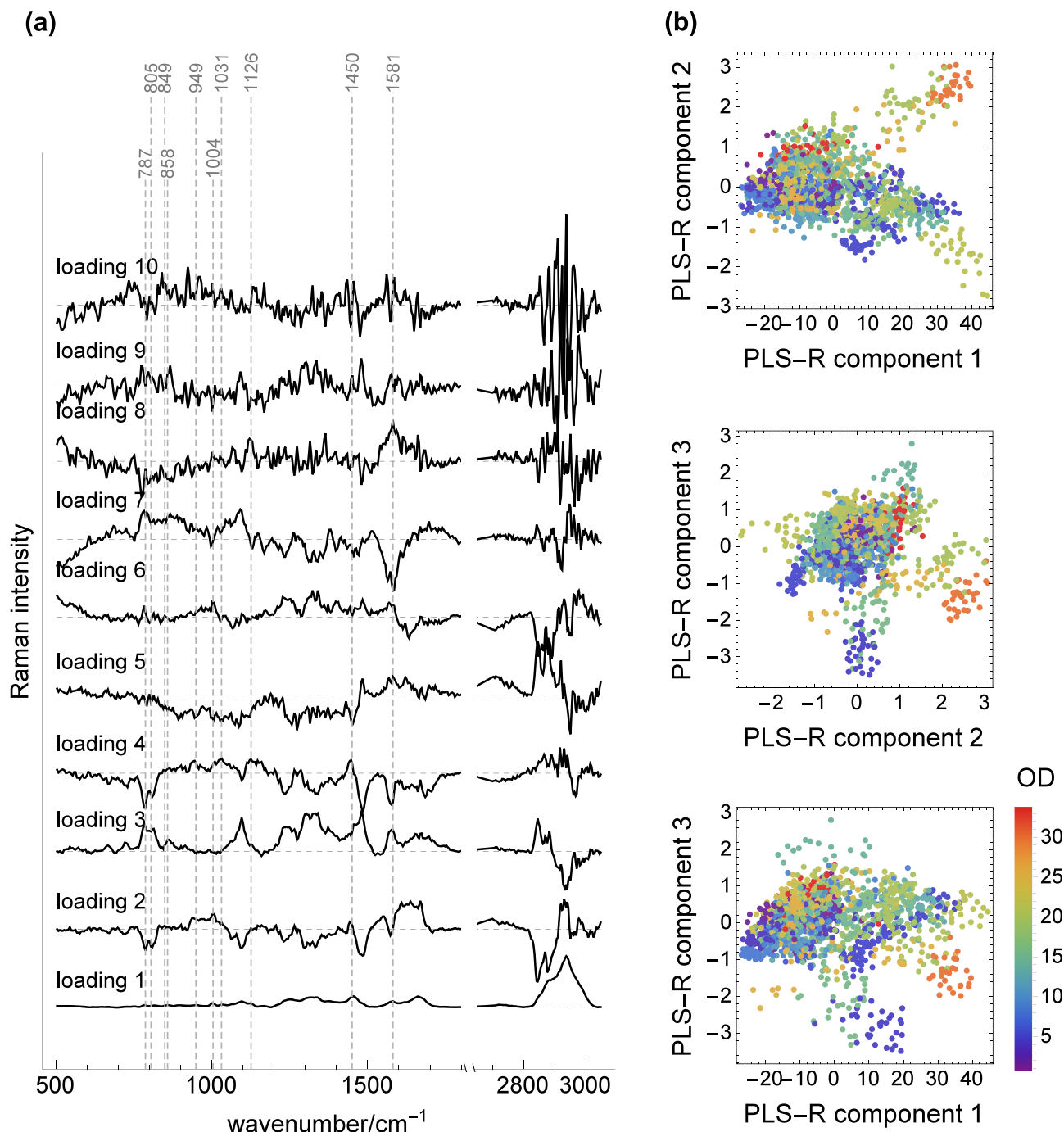


**FIGURE 3** Loadings and score plots of partial least square regression (PLSR) for whole data set showing the 10 PLSR components. The loadings (left) reveal negative correlation of the Raman bands at  $787\text{ cm}^{-1}$  and  $804\text{--}809\text{ cm}^{-1}$  (nucleic acids) and a positive correlation of the bands at  $849$ ,  $949$ ,  $1031$ , and  $1126\text{ cm}^{-1}$  (carbohydrates) and the phenylalanine band at  $1004\text{ cm}^{-1}$  (proteins) with the optical density (OD) values from the crystal violet test is seen. The score plots with the first three PLSR loadings (right) can achieve a slight separation of the Raman data according to the OD values from the crystal violet test (especially PLSR component 2). The color codes the OD values from crystal violet test

production of RNA leading to a reduction of the RNA band intensity at  $805\text{ cm}^{-1}$  and the purine bases band intensity at  $787\text{ cm}^{-1}$ . In agreement, Carey et al.<sup>[20]</sup> reported an absence of the RNA band at  $810\text{--}815\text{ cm}^{-1}$

in *E. coli* biofilm, whereas it was well present in its planktonic counterpart. Therefore, the result of the PLSR can be explained also by a downregulated RNA production associated with an increased biofilm

production. Possible DNA is likely to be washed away during sample preparation. The band at  $1581\text{ cm}^{-1}$  also displayed a decreased relative intensity in high biofilm producer strains (Figures 1 and S5). A relative decrease of the nucleic acid band intensities was generally also observed in biofilms from other common clinical bacterial species.<sup>[16,17,23,25]</sup>

Another prominent band positively correlated with the OD values from crystal violet test is the phenylalanine band at  $1004\text{ cm}^{-1}$ . Proteins beside carbohydrates and extracellular DNA are the third main component in the bacterial biofilm. A recent review that summarized current studies on biofilms using Raman spectroscopy and surface-enhanced Raman spectroscopy suggested that the phenylalanine ring-breathing band could be used as protein signature band for biofilm formation.<sup>[43]</sup> Thus, it might be a good indicator for detection of protein-based biofilms. Indeed, *S. aureus* is known to either produce PIA-based biofilms or protein-based biofilms.<sup>[5]</sup> Therefore, our results indicate that the increase in the phenylalanine band might be a good indicator for biofilm production capability in protein-based biofilms that lack PIA. An increase in the phenylalanine band was also found in *Pseudomonas sp.* strain ADP biofilm<sup>[21]</sup> and *P. aeruginosa* biofilm<sup>[16]</sup> compared with the planktonic form.

It has to be noted that the cultivation conditions for the Raman experiment are not identical to the crystal violet assay. We used much shorter cultivation times for the Raman experiment to detect metabolic changes in the bacterial cells in preparation of biofilm formation. Ideally, fresh bacterial samples directly isolated from the patient should have been used, which was—unfortunately—not possible during sample collection. In this study, bacteria from blood agar plates were used. Thus, our interpretation of detecting EPS molecule signatures in the Raman spectra is based on the assumption that bacteria in the liquid culture might have already started producing molecules that are used for building up the EPS. Two observations are supporting our hypothesis: first, the EPS can make up to 10 times the mass of bacterial cells,<sup>[44]</sup> thus making high production and secretion of EPS molecules necessary that might start already before attachment of the bacteria to a surface and might be necessary for the attachment process itself. Second, it is generally accepted that strong shear forces promote biofilm formation.<sup>[45]</sup> The bacterial cultures used in this study were shaken at high speed generating strong shear forces as well and might therefore have induced synthesis of molecules involved in biofilm formation. This is supported by a recent study showing that biofilm formation is increased in *S. epidermidis* patient isolates from

environments with high shear stress such as catheters and that these strains showed enhanced PIA production under high shear forces in vitro.<sup>[46]</sup>

A study by Rebrosova et al.<sup>[47]</sup> showed that it is possible to use Raman spectroscopy for differentiation of biofilm-positive and biofilm-negative *S. epidermidis* and *Candida parapsilosis* strains, respectively, with high accuracy. Similar to our study, they tested the strains for biofilm formation with a crystal violet test and used this information (biofilm positive or negative) for classification of the strains in different machine learning methods. Interestingly, the biofilm prediction was successful although Raman spectra acquisition was also not done on the strains grown as biofilm. Instead, Raman spectra were measured from colonies grown for 24 h on agar plates. This supports the results from our study where we have used planktonic bacteria instead of cultivated biofilms.

## 5 | CONCLUSION

The study demonstrates that Raman spectroscopy gives the possibility to be applied also as a fast predictable method for biofilm formation in vitro without prior bacterial cultivation with biofilm production. The (weak) correlation seen in leave one spectrum out scores of predicted OD against real OD as well as in the score plots from the whole data set together is a very promising indication of this. For validation, more data have to be collected in future. Combined with the rapid analysis of antibiotic susceptibility and bacterial species prediction, this technology gives the possibility to identify further important clinical features of bacterial strains isolated from patients with bacteremia, prosthesis, or wound infection. It therefore could estimate the risk of a patient if the strain responsible for the infection could form a biofilm or not. This would help to prevent biofilm formation by using antibiotics that are known to efficiently penetrate biofilms and might help to avoid removal of implants for the purpose of in vivo diagnostics and therapy.


## ACKNOWLEDGEMENTS

This work was funded by the Bundesministerium für Bildung und Forschung (BMBF) via the Center for Sepsis Control and Care (FKZ 01EO1502). We furthermore acknowledge support by the Leibniz Association via the Leibniz ScienceCampus InfectoOptics (W8/2018) and by the European Union via the Horizon 2020 research and innovation program under grant agreement no. 861122 (IMAGE-IN).

**DATA AVAILABILITY STATEMENT**

Data are available upon request.

**ORCID**

Lorena Tuchscherer  <https://orcid.org/0000-0002-9328-5302>

Ute Neugebauer  <https://orcid.org/0000-0002-7593-6132>

**REFERENCES**

- [1] A. Sakr, F. Bregeon, J. L. Mege, J. M. Rolain, O. Blin, *Front. Microbiol.* **2018**, *9*, 2419.
- [2] H. C. Flemming, J. Wingender, U. Szewzyk, P. Steinberg, S. A. Rice, S. Kjelleberg, *Nat. Rev. Microbiol.* **2016**, *14*, 563.
- [3] W. R. Abraham, *Antibiotics (Basel)* **2016**, *5*, 3.
- [4] C. R. Arciola, D. Campoccia, L. Montanaro, *Nat. Rev. Microbiol.* **2018**, *16*, 397.
- [5] K. Schilcher, A. R. Horswill, *Microbiol. Mol. Biol. Rev.* **2020**, *84*, e00026.
- [6] N. K. Archer, M. J. Mazaitis, J. W. Costerton, J. G. Leid, M. E. Powers, M. E. Shirtliff, *Virulence* **2011**, *2*, 445.
- [7] S. Stepanovic, D. Vukovic, I. Dakic, B. Savic, M. Svabic-Vlahovic, *J. Microbiol. Methods* **2000**, *40*, 175.
- [8] Z. Xu, Y. Liang, S. Lin, D. Chen, B. Li, L. Li, Y. Deng, *Curr. Microbiol.* **2016**, *73*, 474.
- [9] E. Peeters, H. J. Nelis, T. Coenye, *J. Microbiol. Methods* **2008**, *72*, 157.
- [10] C. Staudt, H. Horn, D. C. Hempel, T. R. Neu, *Biotechnol. Bioeng.* **2004**, *88*, 585.
- [11] M. J. Franklin, C. Chang, T. Akiyama, B. Bothner, *Microbiol Spectr* **2015**, *3*(4), MB-0016-2014.
- [12] F. Pantanella, P. Valenti, T. Natalizi, D. Passeri, F. Berlutti, *Ann. Ig.* **2013**, *25*, 31.
- [13] T. F. Bahamondez-Canas, L. A. Heersema, H. D. C. Smyth, *Biomedicine* **2019**, *7*, 34.
- [14] S. Stoeckel, J. Kirchhoff, U. Neugebauer, P. Roesch, J. Popp, *J. Raman Spectrosc.* **2016**, *47*, 89.
- [15] C. Sandt, T. Smith-Palmer, J. Pink, L. Brennan, D. Pink, *J. Appl. Microbiol.* **2007**, *103*, 1808.
- [16] R. N. Masyuko, E. J. Lanni, C. M. Driscoll, J. D. ShROUT, J. V. Sweedler, P. W. Bohn, *Analyst* **2014**, *139*, 5700.
- [17] D. Kusic, B. Kampe, A. Ramoji, U. Neugebauer, P. Rosch, J. Popp, *Anal. Bioanal. Chem.* **2015**, *407*, 6803.
- [18] J. Feng, C. de la Fuente-Nunez, M. J. Trimble, J. Xu, R. E. Hancock, X. Lu, *Chem. Commun.* **2015**, *51*, 8966.
- [19] J. Feng, G. Lamour, R. Xue, M. N. Mirvakliki, S. G. Hatzikiriakos, J. Xu, H. Li, S. Wang, X. Lu, *Int. J. Food Microbiol.* **2016**, *238*, 172.
- [20] P. R. Carey, B. R. Gibson, J. F. Gibson, M. E. Greenberg, H. Heidari-Torkabadi, M. Pusztai-Carey, S. T. Weaver, G. R. Whitmer, *Biochemistry* **2017**, *56*, 2247.
- [21] V. A. Henry, J. L. Jessop, T. L. Peebles, *Anal. Bioanal. Chem.* **2017**, *409*, 1441.
- [22] N. P. Ivleva, P. Kubryk, R. Niessner, *Anal. Bioanal. Chem.* **2017**, *409*, 4353.
- [23] L. Tan, F. Zhao, Q. Han, A. Zhao, P. K. Malakar, H. Liu, Y. Pan, Y. Zhao, *Front. Microbiol.* **2018**, *9*, 1881.
- [24] P. Chen, J. J. Wang, B. Hong, L. Tan, J. Yan, Z. Zhang, H. Liu, Y. Pan, Y. Zhao, *Front. Microbiol.* **2019**, *10*, 2543.
- [25] X. Y. Liu, S. Guo, A. Ramoji, T. Bocklitz, P. Rosch, J. Popp, H. Q. Yu, *Anal. Chem.* **2020**, *92*, 707.
- [26] B. Gieroba, M. Krysa, K. Wojtowicz, A. Wiater, M. Pleszczyńska, M. Tomczyk, A. Sroka-Bartnicka, *Int. J. Mol. Sci.* **2020**, *21*, 3811.
- [27] P. Vega-Dominguez, E. Peterson, M. Pan, A. Di Maio, S. Singh, S. Umapathy, D. K. Saini, N. Baliga, A. Bhatt, *Cell Surf* **2020**, *6*, 100043.
- [28] B. D. Beier, R. G. Quivey, A. J. Berger, *J. Biomed. Opt.* **2010**, *15*, 066001.
- [29] B. D. Beier, R. G. Quivey, A. J. Berger, *AMB Expr.* **2012**, *2*, 35.
- [30] O. Samek, S. Bernatova, J. Jezek, M. Siler, M. Sery, V. Krzyzaneck, K. Hrubanova, P. Zemanek, V. Hola, F. Ruzicka, *J. Biomed. Opt.* **2015**, *20*, 051038.
- [31] L. S. Kriem, K. Wright, R. A. Ccahuana-Vasquez, S. Rupp, *PLoS ONE* **2020**, *15*, e0232912.
- [32] X. Lu, D. R. Samuelson, B. A. Rasco, M. E. Konkel, *J. Antimicrob. Chemother.* **2012**, *67*, 1915.
- [33] G. B. Jung, S. W. Nam, S. Choi, G. J. Lee, H. K. Park, *Biomed. Opt. Express* **2014**, *5*, 3238.
- [34] N. F. Baig, S. J. Dunham, N. Morales-Soto, J. D. ShROUT, J. V. Sweedler, P. W. Bohn, *Analyst* **2015**, *140*, 6544.
- [35] L. Tuchscherer, C. Pollath, A. Siegmund, S. Deinhardt-Emmer, V. Hoerr, C. M. Svensson, M. Thilo Figge, S. Monecke, B. Löffler, *Toxins (Basel)* **2019**, *11*, 135.
- [36] G. A. O'Toole, R. Kolter, *Mol. Microbiol.* **1998**, *28*, 449.
- [37] L. P. Choo-Smith, K. Maquelin, T. van Vreeswijk, H. A. Bruining, G. J. Puppels, N. A. Ngo Thi, C. Kirschner, D. Naumann, D. Ami, A. M. Villa, F. Orsini, S. M. Doglia, H. Lamfarraj, G. D. Sockalingum, M. Manfait, P. Allouch, H. P. Endtz, *Appl. Environ. Microbiol.* **2001**, *67*, 1461.
- [38] U. Neugebauer, U. Schmid, K. Baumann, W. Ziebuhr, S. Kozitskaya, V. Deckert, M. Schmitt, J. Popp, *ChemPhysChem* **2007**, *8*, 124.
- [39] P. Rösch, M. Harz, K.-D. Peschke, O. Ronneberger, H. Burkhardt, A. Schüle, G. Schmauz, M. Lankers, S. Hofer, H. Thiele, H.-W. Motzkus, J. Popp, *Anal. Chem.* **2006**, *78*, 2163.
- [40] S. Stöckel, J. Kirchhoff, U. Neugebauer, P. Rösch, J. Popp, *J. Raman Spectrosc.* **2016**, *47*, 89.
- [41] A. A. Makki, F. Bonnier, R. Respaud, F. Chtara, A. Tfayli, C. Tauber, D. Bertrand, H. J. Byrne, E. Mohammed, I. Chourpa, *Spectrochim. Acta, Part a* **2019**, *218*, 97.
- [42] N. P. Ivleva, M. Wagner, H. Horn, R. Niessner, C. Haisch, *Anal. Bioanal. Chem.* **2009**, *393*, 197.
- [43] S. Kelestemur, E. Avci, M. Culha, *Chemosensors* **2018**, *6*, 5.
- [44] A. Vertes, V. Hitchins, K. S. Phillips, *Anal. Chem.* **2012**, *84*, 3858.
- [45] R. M. Donlan, J. W. Costerton, *Clin. Microbiol. Rev.* **2002**, *15*, 167.
- [46] C. R. Schaeffer, T. N. Hoang, C. M. Sudbeck, M. Alawi, I. E. Tolo, D. A. Robinson, A. R. Horswill, H. Rohde, P. D. Fey, *mSphere* **2016**, *1*(5), e00165-16.
- [47] K. Rebrosova, M. Siler, O. Samek, F. Ruzicka, S. Bernatova, J. Jezek, P. Zemanek, V. Hola, *Future Microbiol.* **2019**, *14*, 509.

- [48] L. Tuchscher, M. Bischoff, S. M. Lattar, M. Noto Llana, H. Pförtner, S. Niemann, J. Geraci, H. Van de Vyver, M. J. Fraunholz, A. L. Cheung, M. Herrmann, U. Völker, D. O. Sordelli, G. Peters, B. Löffler, *PLoS Pathog.* **2015**, *11*, e1004870.

**How to cite this article:** C. Ebert, L. Tuchscher, N. Unger, C. Pöllath, F. Gladigau, J. Popp, B. Löffler, U. Neugebauer, *J Raman Spectrosc* **2021**, *52*(12), 2660. <https://doi.org/10.1002/jrs.6237>

### SUPPORTING INFORMATION

Additional supporting information may be found in the online version of the article at the publisher's website.